Thermoelectricity and electronic properties of Y1-xCexCrB4

Flipo, S.; Rosner, H.; Bobnar, M.; Kvashnina, K.; Leithe-Jasper, A.; Gumeniuk, R.;

Originally published:

May 2021

Physical Review B 103(2021), 195121

DOI: https://doi.org/10.1103/PhysRevB.103.195121

Thermoelectricity and electronic properties of $Y_{1-x}Ce_xCrB_4$

Sever Flipo,[1,2] Helge Rosner,[2] Matej Bobnar,[2] Kristina O. Kvashnina,[3,4] Andreas Leithe-Jasper,[2] and Roman Gumeniuk[1,*]

[1] *Institut für Experimentelle Physik, TU Bergakademie Freiberg, Leipziger Straße 23, 09596 Freiberg, Germany*
[2] *Max-Planck-Institut für Chemische Physik fester Stoffe, Nöthnitzer Straße 40, 01187 Dresden, Germany*
[3] *Helmholtz-Zentrum Dresden-Rossendorf, Institute of Resource Ecology, Bautzner Landstrasse 400, 01328 Dresden, Germany*
[4] *The Rossendorf Beamline at ESRF, CS 40220, 38043 Grenoble Cedex 9, France*

(Dated: March 24, 2021)

Boron rich materials combine chemical stability with refractory properties and consequently are interesting for high temperature thermoelectric applications. Therefore, the magnetic, electrical and thermal transport properties of the $Y_{1-x}Ce_xCrB_4$ series have been investigated here to employ the concept of correlation enhanced thermoelectric properties. Combining X-ray diffraction and energy- or wavelength-dispersive spectrometry, we find a rather narrow stability range of $Y_{1-x}Ce_xCrB_4$, only samples on the Y- and Ce-rich substitution limits (x = 0, 0.05, 0.95, 1) were obtained. Electrical resistivity data show a change from semiconducting (x = 0) to metallic behavior upon Ce substitution ($x \geq$0.95). From magnetic susceptibility measurements and x-ray absorption spectroscopy, we find a temperature dependent intermediate valence state of Ce of about +3.5. However, a fit of the magnetic susceptibility data to the Coqblin-Schrieffer model yields a surprisingly high Kondo-temperature of about 1100 K. Together with the good thermal conductivity for the studied substitution series this impedes a suitable thermoelectric performance. Electronic structure calculations for $YCrB_4$ support its narrow gap semiconducting nature in contrast to previous studies. Surprisingly, its electronic structure is characterized by pronounced van-Hove singularities very close to the Fermi level E_F. They originate from nearly dispersionless Cr $3d_{z^2-r^2}$ derived bands in a large part of the Brillouin zone, suggesting the appearance of electronic instabilities upon rather small electron doping into these states.

I. INTRODUCTION

Thermoelectric (TE) materials, which can convert heat into electricity became an object of special scientific interest in the past few decades. Such a research is motivated by the facts that solid-state energy conversion is suitable for harvesting waste heat completely environmental friendly under various technical conditions. However, beside these clear advantages thermoelectrics are very demanding in optimization. As it is known, their efficiency, which is given as dimensionless figure of merit $ZT = S^2T\sigma/\kappa$, is expected to be high for materials revealing at the same time good electrical (σ) and poor thermal (κ) conductivities (S and T in the formula stand for Seebeck coefficient and temperature, respectively). The physically opposing requirements of high σ and low κ are a challenging obstacle for the achievement of the technically desired high ZT.

Another crucial issue for technical applications are the restricted working temperature ranges for specific materials. For instance, such prominent thermoelectrics as Bi_2Te_3, PbTe and SiGe reveal the best efficiency (i.e. $ZT \approx 1$) at 300-500 K, 600-800 K and 1100-1300 K, respectively [1, 2]. With respect to high temperature (HT) applications, intermetallic boron-rich materials (refractory and chemically stable compounds containing rare-earth-, transition metals as well as > 50 at. % boron) seem to be promising. Only few such materials have been discovered up to now and some of them are reported to be narrow gap semiconductors [3, 4] potentially revealing high TE efficiency [5]. A family of promising borides exhibits layered structures crystallizing with orthorhombic $YCrB_4$ structure type [6, 7]. For this class of materials, electronic structure calculations indicated energy gaps of ∼0.2-0.5 eV for $YCrB_4$ [8], $YMnB_4$ [9], $YMoB_4$ and YWB_4 [10]. However, further experimental investigations performed on $YMoB_4$ and its carbon and iron doped variants revealed their electrical transport characteristics, given as a power factor $PF = S^2\sigma \approx 10^{-4}$ W m^{-1} K^{-2} [11], still too low for a reasonably efficient TE material. For the improvement of the TE performance of 1:1:4 borides, a simple manipulation of the charge carrier concentration by electron or hole doping is unlikely to be sufficient.

Another potentially promising way to improve the TE properties might be the introduction of correlation effects by Ce substitution on the Y site. A classical example, where this approach is working is $CePd_3$ - a dense Kondo system with Ce-ions in the intermediate valence state (IVS) [12]. This system is characterized by an enhanced Kondo temperature T_K = 300 K, which is proportional to the Ce-4f spin fluctuation rate and thus, to the strength of the hybridization of 4f electrons with conduction states [13]. This leads to the appearance of unoccupied Ce-4f states slightly above the Fermi level (E_F), which can become partially populated [14, 15]. As a result of such electron correlations, atypically high values of the Seebeck coefficient of $S \approx 115\mu$V K^{-1} at room temperature were observed, resulting in unexpectedly good TE efficiency $ZT \sim 0.2$ for $CePd_3$ [16].

In $CeCrB_4$, isotypic to $YCrB_4$, Ce seems to be in an IVS since its unit cell volume deviates strongly from the linear dependence of other volumes of the isostructural RCrB$_4$ borides in an Iandelli plot [17]. In light of the above mentioned Ce $4f$ physics, we attempt in this work a systematic study of the Ce substitution series in $YCrB_4$. Here we report on the crystal structures, magnetic properties as well as electrical and thermal transport in the $Y_{1-x}Ce_xCrB_4$ series. Despite the chemical similarity between the ternary $YCrB_4$ and $CeCrB_4$ borides, only limited solubility of Ce in the Y-compound and vice versa is observed (*i.e.* $x = 0$, 0.05, 0.95, 1) which might point to an IVS of Ce in the substitution series. Since previously published electronic structure calculations for the undoped YTB_4 compounds (T = Cr, Fe, Co, Mn, Mo, W, Re) were nor conclusive with respect to details of the structure properties relations [8, 9, 10, 11, 14] in particular the influence of the crystallographic boron positions, we also perform density functional (DFT) calculations to obtain more specific information.

II. EXPERIMENTAL

Samples with the nominal composition $Y_{1-x}Ce_xCrB_4$ ($x = 0, 0.05, 0.10, 0.15, 0.85, 0.90, 0.95, 1$) were prepared from Y pieces (Lamprecht 99.9 %), Ce rod (Chempur 99.9 %), Cr pieces (Chempur 99.99 %) and B crystalline powder (Alpha-Aesar 99.999 %). In order to have a single button, the pieces were firstly carefully melted together, under Ar-atmosphere on a water-cooled copper hearth. To ensure homogeneity they were then re-melted several times. The mass loss in this process was below 2 wt. %. Further heat treatment for 7 days was performed in W-crucibles, which were sealed in Ta-tubes at 1570 K. All handling was carried out in Ar-filled glove boxes (MBraun, $p(O_2/H_2O) \leq 1$ ppm).

Differential scanning calorimetry was performed with a DSC NETZSCH 404F1 on ternary $YCrB_4$ and $CeCrB_4$ in temperature ranges of 300 2070 K. Refractory $YCrB_4$ reveals no thermal effects neither in warming nor in cooling curves, which suggests stability of the studied samples in the temperature range mentioned above. The $CeCrB_4$ boride shows two rather weak signals in the warming cycle at 1580 K and 1585 K, which would indicate a peritectic decomposition of the studied phase in this temperature range. For this reason (to be able to compare unit cell parameters of the whole $Y_{1-x}Ce_xCrB_4$ series) the annealing temperature was chosen to be 1570 K.

All obtained samples were powdered, stress annealed at 1570 K for 2 hours in Ta-tubes under Ar-atmosphere and further characterized by powder X-ray diffraction (PXRD) on a Huber G670 imaging plate Guinier camera equipped with a curved Ge (111) monochromator [$CuK_{\alpha1}$ ($\lambda = 1.54056$ Å) or $CoK_{\alpha1}$ ($\lambda = 1.78897$ Å)]. Phase analysis and indexing were done using WinXPow program package [18]. The indexing of all PXRD patterns as well as further crystal structure refinements were performed using WinCSD program package [19].

For microstructural studies, a small piece of each compound was embedded in a conductive resin and then polished. The obtained surface was investigated using a light-optical microscope (Zeiss Axioplan 2) and a scanning electron microscope (Jeol JSM - 7800F). The chemical composition was analysed by means of energy dispersive X-ray spectroscopy (EDXS) (Quantax 400 EDXS system, Bruker) and wavelength dispersive X-ray spectroscopy (WDXS) (SX 100, Cameca) with CrB, YB_4 and CeB_4 as references. The obtained compositions are in good agreement with the nominal ones (Table. I).

HERFD-XAS experiments were performed at MARS beamline of SOLEIL in France. The incident energy was selected using the $\langle 111 \rangle$ reflection from a double Si crystal monochromator. HERFD-XAS spectra were measured using an X-ray emission spectrometer [20] at 90° horizontal scattering angle. Sample, analyzer crystal and photon detector (avalanche photodiode) were arranged in a vertical Rowland geometry. The Ce HERFD-XAS spectra at the L_{III} edge were obtained by recording the maximum intensity of the Ce$L_{\alpha1}$ emission line (4839 eV) as a function of the incident energy. The emission energy was selected using the $\langle 400 \rangle$ reflection of one spherically bent Si crystal analyzer (with $R = 1$ m) aligned at a 71° Bragg angle. The size of the beam at the sample was 400 mm horizontal times 200 mm vertical. A combined (incident convoluted with emitted) energy resolution of 1.4 eV was obtained, as determined by measuring the FWHM of the elastic peak. Samples for the HERFD-XAS measurements were sealed with single kapton confinement.

The magnetic susceptibility was measured in the temperature range 1.8 - 400 K in external fields between 0.1 and 7 T on a SQUID magnetometer (MPMS-XL7, Quantum Design). At low temperature (4 350 K), the electrical resistivity, Seebeck coefficient, thermal conductivity were measured simultaneously with TTO-option on the Physical Property Measurement System (PPMS, Quantum Design). At higher temperature (300 1070 K), the electrical resistivity and Seebeck coefficient were measured on a ZEM-3 device (Ulvac-Riko). The HT thermal conductivity was estimated from: $\kappa(T) = D(T) \cdot c_p(T) \cdot \delta(T)$, where $D(T)$ is thermal diffusivity [measured using the Laser Flash Method (LFA 457 MicroFlash, Netzsch)], $c_p(T)$ is the specific heat [obtained on a differential scanning calorimeter (DSC 8500, PerkinElmer)] and $\delta(T)$ is the density (is assumed to be a constant [i.e. volumetric lattice expansion ∼0.9 % at 623 K] with an average compaction of 97 %).

Relativistic density functional (DFT) electronic structure calculations were performed using the full-potential FPLO code [21], version fplo18.00-52. For the exchange-correlation potential, within the linear density approximation LDA) the parametrization of Perdew-Wang [PW] and for the general gradient approximation (GGA), the parametrization of Perdew-Burke-Ernzerhof [22] were chosen. To obtain precise band structure information, the calculations were carried out on a well converged

mesh of 1724 k-points (6×12×24). The atomic positions were optimized to minimize the total energies with lattice parameters fixed to the experiment.

III. RESULTS AND DISCUSSION

A. Electronic structures

Owing to the previous inconclusive results for the electronic structure of $YCrB_4$, the strong dependence on structural details and the deviation of $CeCrB_4$ in the Iandelli plot (strong volume reduction compared to the $4f$ series [17, 23]) we try to find out in a first step whether these compounds are intrinsically metals or semiconductors.

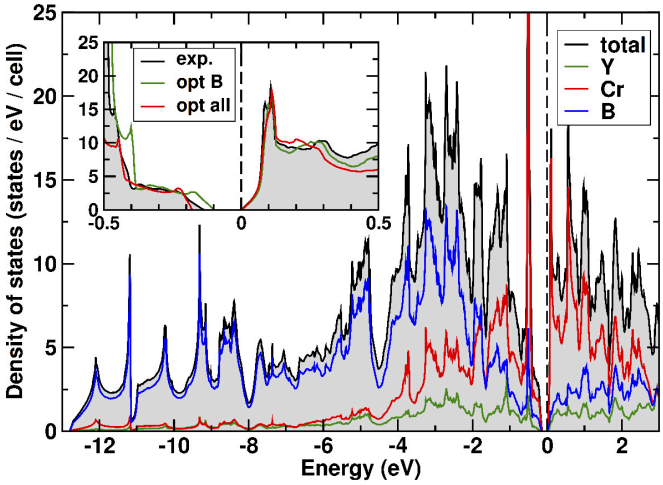

FIG. 1. (Color online) Calculated total and atom resolved partial density of states of $YCrB_4$. The Fermi level is at zero energy (dashed line). The inset shows the energy window near the Fermi level for the experimental structure (exp), relaxed atomic B positions (opt B) and the fully relaxed structure (opt all).

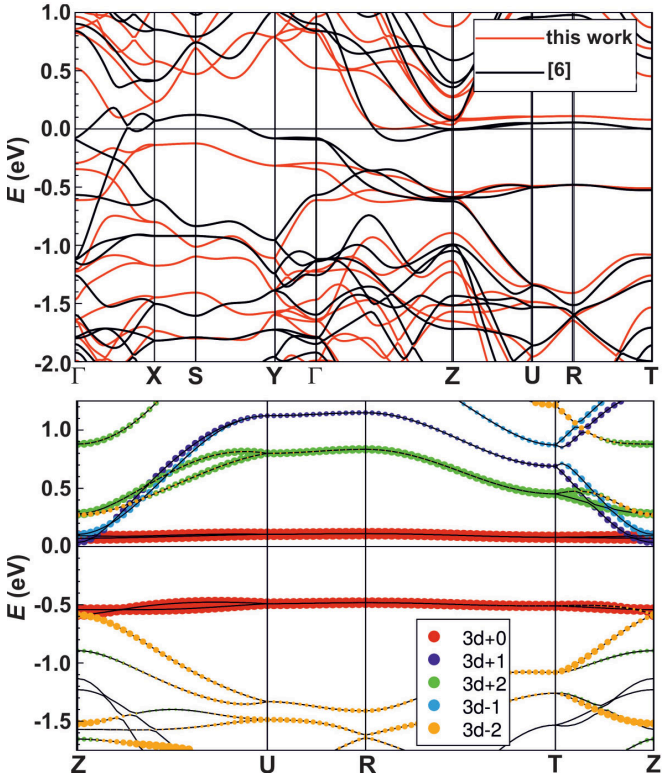

FIG. 2. (Color online) Calculated band structure of $YCrB_4$ near the Fermi level E_F at zero energy. The high symmetry points are denoted as follows: Γ[000], X[100], S[110], Y[010], Z[001], U[101], R[111], T[010] in units of [π/a, π/b, π/c]. The upper panel shows a comparison of the band dispersion for the crystal structure of this work (red lines) with the structure from Kuzma et al. (see Ref. [6], black lines). In contrast to the insulating behavior of the former (compare also Fig. 1) in the latter the bands near EF are slightly shifted against each other, resulting in metallic behavior. The lower panel shows the Cr 3d orbital character for the bands near E_F. The m quantum numbers +0, +1, +2, -1, -2 stand for the $3z^2 - r^2$, xz, $x^2 + y^2$, yz, xy orbitals, respectively.

The electronic density of states (DOS) for $YCrB_4$ is shown in Fig. 1. The valence band is rather broad (about 13 eV) due to the strong hybridization of Cr $3d$ and B $2p$ states. At higher energies above -2 eV the valence band is dominated by Cr states, at energies below -2 eV by B states. For the experimental crystal structure, we find insulating behavior of the compound with a narrow gap of about 140 meV. This gap is of indirect nature (see Fig. 2 upper panel). Surprisingly, using the previously published structural data of Kuzma et al. [6] we find a metallic solution (see Fig. 2 upper panel) since the electron and the hole band are shifted by about 300 meV with respect to each other. On a larger energy scale, the valence band for both crystal structures is very similar (not shown).

The different behavior with respect to the metallicity can be related to the exact B positions, which are intrinsically difficult to determine by X-ray diffraction in the presence of heavy atoms. From the DFT calculations, the new crystallographic data presented in this work are strongly favored by 330 meV per formula unit compared to the structure of Kuzma et al. [6]. Relaxing the B positions for our crystallographic data with respect to the total energy yields only small changes. Depending on the kind of relaxation, all atoms or B atoms only, the electronic gap varies by about ±40 meV (see inset Fig. 1), thus the compound is always exhibiting insulating nature.

For $CeCrB_4$, the correlated nature of the $4f$ electron prohibits a straight forward DFT calculation of its electronic structure. However, to estimate the influence of the considerably larger lattice parameters of the Ce compound compared to the Y system, we exclude the $4f$ level from the valence band in our calculation. As expected, the larger interatomic distances lead to a reduction of the overall valence band width (see Fig. S1). Surprisingly,

the gap at E_F, present in $YCrB_4$, completely disappears and we obtain a sizeable DOS at E_F (see Fig. S1). The closure of this gap is robust with respect to the exact B positions. Relaxing these parameters with respect to the calculated total energy even leads to a further increase of the DOS(E_F). Since there is no other gap like feature above E_F (see Fig. S1), a contribution from non-localised $4f$ electrons is unlikely to induce a non-metallic state for $CeCrB_4$. However, regarding the correlated nature of $4f$ states in general, this calculational result needs experimental justification. Nonetheless, this result suggests that a partial replacement of Y by Ce might result in more promising thermoelectic properties than in the ternary $CeCrB_4$, envisioning a diluted Kondo-like scenario with a gap or a small DOS at E_F and correlated $4f$ states close to E_F.

Independent from the question of metallicity, a very interesting and prominent feature in the electronic structure of $YCrB_4$ are the narrow peaks near the Fermi level (see Fig. 1). The origin of these singularities are two bands that are nearly dispersionless for a large part of the Brillouin zone (see Fig. 2 upper panel, for the path Z-U-R-T). To elucidate the character of these states we plotted their orbital character for this part of the Brillouin zone (see Fig. 2 lower panel). We find that these states originate predominantly from the Cr $3d$ $z^2 - r^2$ orbital. This could be of particular interest, since one would expect that these out-of plane states are robust against substitution at other sites than Cr. If a large enough number of charge carriers can be introduced chemically, one would arrive at a very high metallic DOS at the Fermi level which certainly should drive an electronic instability. From our results, electron doping seems to be the method of choice since the Cr $3d_{z^2-r^2}$ singularity lies directly above the Fermi level (see inset Fig. 1).

B. Phase formation and crystal structure

The strongest peaks in the powder X-ray diffraction patterns (PXRD) of $Y_{1-x}Ce_xCrB_4$ samples with x = 0, 0.05, 0.95 and 1 (in the inset to Fig. 3 selected regions of these PXRDs are depicted) can be indexed in the space group (SG) *Pbam*. The unit cell parameters are presented in Table I. However, the specimens from this series with Ce-content x = 0.10, 0.15, 0.50, 0.85 and 0.90 were found to be multi-phase (*i.e.* containing simultaneously $YCrB_4$ and $CeCrB_4$ phases, see Fig. S2). Their unit cell volumes strongly deviate from a linear Vegard-like dependence [24, 25] (Fig. 3) assuming complete mutual substitution of Y and Ce atoms in $YCrB_4$ and $CeCrB_4$ borides. Thus, we have to conclude that the solubility of the fourth component in the ternaries $YCrB_4$ and $CeCrB_4$ is unexpectedly small indicating the importance of other factors in addition to the atomic-size factor [26]. This limited solubility [27, 28, 29] could be related to the strong differences in the valences of Ce (*i.e.* ∼+3.5) and of Y (*i.e.* +3) together with the concomitant size mismatch. For more details see discussion below.

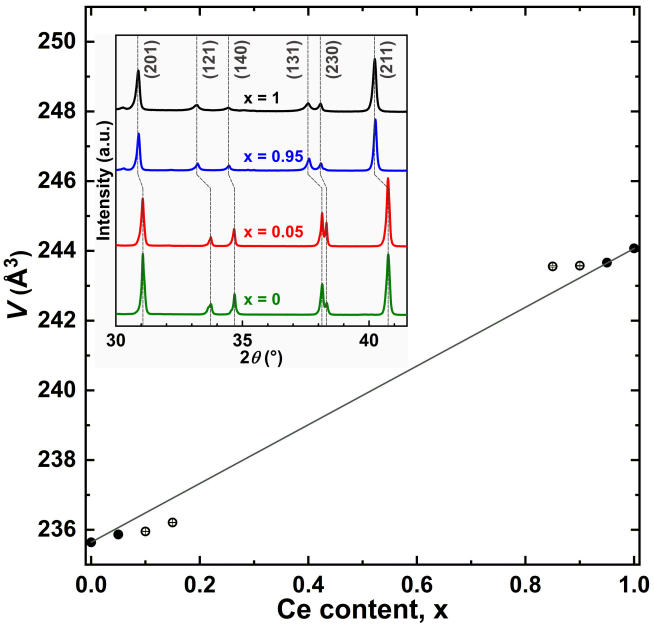

FIG. 3. (Color online) Dependence of the unit cell volume vs Ce-content x in the $Y_{1-x}Ce_xCrB_4$ series. Full circles correspond to the single-phase samples, while empty circles stay for multiphase one. Inset: Powder XRD patterns together with indexing to unit cell parameters given in Table I for the single phase $Y_{1-x}Ce_xCrB_4$.

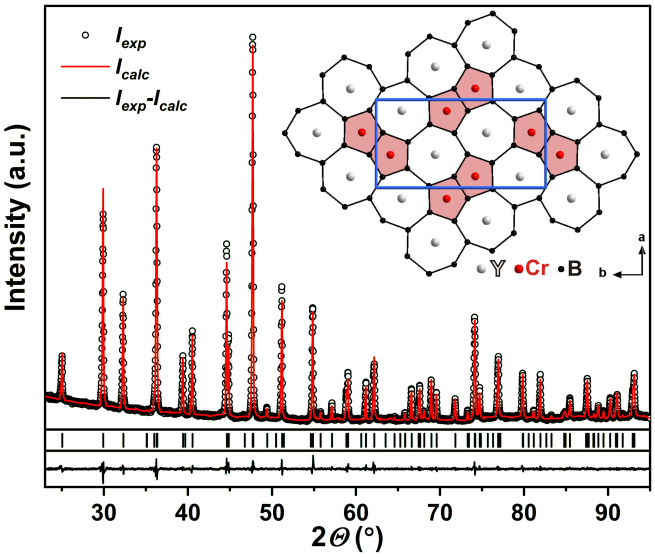

FIG. 4. (Color online) Experimental, theoretically calculated and differential profiles for $Y_{0.95}Ce_{0.05}CrB_4$. Inset shows condensed heptagonal and pentagonal B-rings together with Y- and Cr-atoms at their centres in the structure of the $YCrB_4$ type (for crystallographic details see Tables I and S1)

To refine the crystal structures of $Y_{1-x}Ce_xCrB_4$ (x = 0, 0.05, 0.95, 1) the starting structural model of the $YCrB_4$ type [6] has been used. The crystallographic details of the performed Rietveld refinements are collected

TABLE I. Crystallographic and physical properties data for $Y_{1-x}Ce_xCrB_4$ ($YCrB_4$ structure type, space group $Pbam$, $Z = 4$).

Compound	$YCrB_4$	$Y_{0.95}Ce_{0.05}CrB_4$	$Y_{0.05}Ce_{0.95}CrB_4$	$CeCrB_4$
Crystallographic data				
WDX composition	$Y_{0.96(3)}Cr_{0.93(3)}B_{4.11(10)}$	$Y_{0.96(3)}Ce_{0.04(3)}Cr_{0.98(3)}B_{3.97(10)}$	$Y_{0.05(3)}Ce_{0.95(3)}Cr_{0.96(3)}B_{4.04(10)}$	$Ce_{0.93(3)}Cr_{0.95(3)}B_{4.12(10)}$
a (Å)	5.9368(4)	5.9359(2)	5.9684(3)	5.9707(5)
b (Å)	11.4695(8)	11.4704(4)	11.5443(7)	11.5477(1)
c (Å)	3.4606(2)	3.4642(2)	3.5364(2)	3.5400(3)
V (Å^3)	235.64(5)	235.87(3)	243.67(4)	244.07(6)
Calc. density, ρ (g cm^{-3})	5.19(1)	5.25(1)	6.34(1)	6.40(1)
R_I/R_P	0.074/0.156	0.050/0.111	0.061/0.132	0.066/0.147
Diffraction system	Guinier Camera G670			
Radiation/λ (Å)	$CuK_{\alpha1}$/1.54056	$CoK_{\alpha1}$/1.78897	$CuK_{\alpha1}$/1.54056	$CuK_{\alpha1}$/1.54056
2θ range(°)/step(°)	20-100/0.005			
Magnetism				
$\chi_0 \times 10^{-5}$ (emu mol^{-1})	+3.8(1)	+6.7(1)		+56(1)
$\mu_{\rm eff}$ ($\mu_{\rm B}$)		0.35(3)		0.60(4)
Electrical resistivity and power factor				
ρ_0 ($\mu\Omega$ cm)			17.6(9)	4.05(3)
ρ^{300} ($\mu\Omega$ cm)			116	108
RRR ($\mu\Omega$ cm)			6.7	26.7
$PF_{\rm max}$ (μW cm^{-1} K^{-2}) at [T (K)]	2.23 [375]	8.91 [422]	0.52 [707]	0.46 [613]

in Table I, while obtained atomic coordinates and displacement parameters for the studied borides are presented in Table S1. For $YCrB_4$ we find slightly different boron atomic parameters compared to the previous investigation [6]. The typical theoretical and differential profiles (on the example of $Y_{0.95}Ce_{0.05}CrB_4$) are depicted in Fig. 4. The measured 2θ-range (*i.e.* $2\theta_{\rm max}$ for Guinier Camera G670 is of 100°) do not allow to reliably refine the occupational parameters for Y-Ce statistical mixtures as well as displacement parameters of light B-atoms (Table S1). Nevertheless, the relatively low reliability R-factors nicely confirm the correctness of the chosen structural model.

Since the structural peculiarities of the $YCrB_4$ type and its relationship with other structures have been widely discussed in the literature [6, 30, 31], we only mention here that this structure consists of two planar layers. The layer at $z = 1/2$ is composed of condensed pentagonal and heptagonal rings built by B-atoms, while the layer at $z = 0$ is consisting of Y/Ce- and Cr-atoms (inset to Fig. 4). Similar to earlier reports [30, 31] the interatomic distances (not shown) in the refined structures are close to the sums of the atomic radii of the elements given in Ref. [32]. However, the small variation in the boron parameters significantly influences the electronic structure as has been outlined above and thus, the physical properties (see below).

C. X-ray absorption spectroscopy (XAS)

XAS data of $Y_{1-x}Ce_xCrB_4$ ($x = 0.05, 0.95, 1$) borides measured at the $CeL_{\rm III}$ edge in absorption mode are compared with high resolution spectra of reference compounds $Ce(NO_3)_3$ (Ce^{+3}, $4f^1$ configuration) and CeO_2 (Ce^{+4}, $4f^0$ configuration) in Fig. 5 (all measurements were performed at room temperature). The Ce^{+3} system is characterized by only one white line centred at ∼5727 eV, while Ce^{+4} shows two groups of features at ∼5730 eV and ∼5740 eV. As one can see from Fig. 5, spectra of $CeCrB_4$ and $Y_{1-x}Ce_xCrB_4$ ($x = 0.05, 0.95$) borides are characterized by two broad white lines, which occur at nearly the same energy positions as the groups of features in the spectrum of CeO_2. Also, the full widths at the half of the maxima (FWHM) of the peaks in the borides spectra as well as their intensities are almost the same as those of two white lines centred at ∼5730 eV and another two at ∼5740 eV in XAS of CeO_2.

A deconvolution of the XAS spectra shows that the mean valence ν of Ce is 3.51(2), 3.55(2) and 3.43(2) for $CeCrB_4$, $Y_{0.05}Ce_{0.95}CrB_4$ and $Y_{0.95}Ce_{0.05}CrB_4$, respectively.

D. Magnetic susceptibility

Temperature dependencies of magnetic susceptibilities $\chi(T)$ and reciprocal $\chi^{-1}(T)$ for $Y_{1-x}Ce_xCrB_4$ ($x = 0$, 0.05, 0.95, 1) are depicted in Figs. 6 and S3, respectively.

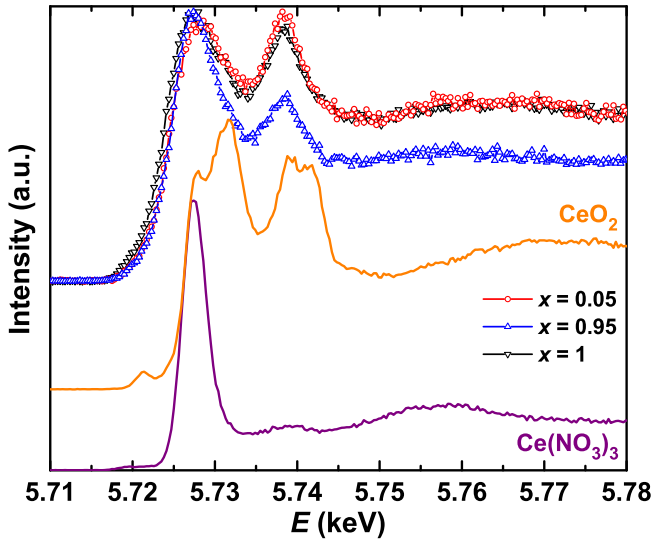

FIG. 5. (Color online) X-ray absorption spectra of $Ce(NO_3)_3$, CeO_2 and $Y_{1-x}Ce_xCrB_4$ borides at CeL_{III} edge.

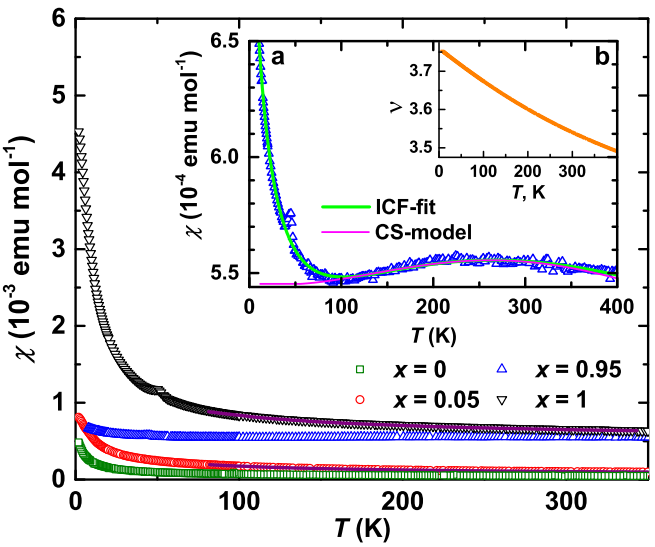

FIG. 6. (Color online) Temperature dependence of the magnetic susceptibility of $Y_{1-x}Ce_xCrB_4$ borides together with CW-fits (purple lines). Inset a: magnetic susceptibility of $Y_{0.05}Ce_{0.95}CrB_4$ together with a fit to the ICF model and prediction of Coqblin-Schriffer for $J = 3/2$ multiplet. Inset b: temperature dependence of the valency ν for $Y_{0.05}Ce_{0.95}CrB_4$ deduced from the ICF-fit. Note: The anomaly at ∼50 K is due to a small trace of oxygen impurity in the liquid Helium used at the time of the measurements.

Unexpectedly, $\chi(T)$ of $YCrB_4$ is found to reveal a strong curvature with relatively large $\chi_0 = 3.8{\times}10^{-5}$ emu mol^{-1} (Table. I). Such a discrepancy with the theoretical calculations, indicating $YCrB_4$ to be a semiconductor with no DOS at E_F, can be explained with the presence of some minor paramagnetic impurities in the studied sample (see discussion below and Figs. S3 and S4). Incorporation of Ce in the structure of $YCrB_4$ leads to the gradual increase of $\chi(T)$ with increasing Ce-content. Interestingly, $\chi^{-1}(T)$ of $Y_{1-x}Ce_xCrB_4$ ($x = 0.05, 0.95, 1$) are linear in the narrow temperature range of 250-350 K (Fig. S5). Therefore, the magnetic susceptibilities of the samples with $x = 0.05$ and 1 were fit to a modified Curie law (Curie + temperature independent term) for $T > 100$ K. The obtained values of the χ_0 and effective magnetic moments are presented in Table. I. Small $\mu_{\rm eff}$ (due to Ce^{+3} contribution) increasing with x correlate well with the predominantly $4f^0$ state of Ce-atoms (i.e. Ce^{+4}) observed in XAS. No phase transitions are seen in the susceptibilities of $Y_{1-x}Ce_xCrB_4$ ($x = 0, 0.05, 1$) down to 1.8 K.

The magnetic susceptibility of $Y_{0.05}Ce_{0.95}CrB_4$ shows some special features comparing to other the $Y_{1-x}Ce_xCrB_4$ borides. It reveals a broad maximum centered at ∼250 K, then decreases down to ∼100 K and finally slightly increases below this temperature. Such a behavior is a signature of a temperature dependent intermediate valence state of Ce-atoms in an intermetallic compound and could point towards electron correlation effects [16, 33, 34].

Kondo systems with large characteristic energy are frequently characterized by a broad maximum in $\chi(T)$ as well. Therefore, we compared the susceptibility of $Y_{0.05}Ce_{0.95}CrB_4$ with the Coqblin-Schrieffer (CS) model calculated by Rajan [35].

Interestingly, in the temperature range from 100 to 400 K the best description of $\chi(T)$ is observed for $J = 3/2$ instead of the $J = 5/2$ multiplet expected for Ce^{3+} (scaling energy $T_0 = 1321$ K; see inset (a) to Fig. 6). This discrepancy can be understood due the fact that the CS-model does not take into account crystal electric field (CEF) splitting effects [35]. The CEF splitting scheme for $Y_{0.05}Ce_{0.95}CrB_4$ is likely of rather complex character, because of the low point symmetry of the Ce position. The fact that the data fit better to a $J = 3/2$ instead of the $J = 5/2$ multiplet are consistent with this idea. Similar effects were reported for $Ce_xLa_{1-x}Cu_{2.05}Si_2$ [36], $YbCu_{5-x}Ag_x$ [37] and YbCuAl [38], where in the case of the Yb-containing compounds $J = 5/2$ multiplets instead of $J = 7/2$ provided good fits to the data. Here it should be noted, that the CEF splitting can be estimated using low-temperature field dependent specific heat capacity and/or inelastic neutron scattering only if it is of different order of magnitude compared to the strength of the Kondo interaction. Otherwise, both methods could fail in the estimation of the needed parameters, as it was observed for the YbCuAl IV system [39].

Despite the discrepancy with the degeneracy of the $Y_{0.05}Ce_{0.95}CrB_4$ system, we converted the scaling energy T_0 into a Kondo temperature (in its high-T definition) according to $T_K = 2\pi T_0 W_J/(2J+1) = 1107$ K, where $W_{3/2} = 0.5335$ is the Wilson number that relates χ_0 to T_K [40]. The Kondo temperature $T_K = 1107$ K estimated for $Y_{0.05}Ce_{0.95}CrB_4$ in this way is by a factor of about 4 larger than the T_K observed for $CePd_3$ ($T_K =$

300 K [16]). This is consistent with the fact that neither Kondo correlations nor the anticipated improvement of the TE performance could be observed for $T < T_K$ in the transport properties (see below).

Trying to deduce the Ce-valence from the magnetic susceptibility measurements we described the broad maximum in $\chi(T)$ by applying the simplified two-level interconfiguration fluctuation model (ICF) [41] (*i.e.* neglecting the complicated Ce^{+3} ions $J = 5/2$ muliplet):

$$\chi_{ICF}(T) = N_A \mu_{eff}^2 \frac{1 - n_{eff}}{k_B(T + T_{sf})} \quad (1)$$

where n_{eff} is the fractional occupation of the +4 state, given as:

$$n_{eff} = \frac{1}{1 + 6\exp[-E_{ex}/k_B(T + T_{sf})} \quad (2)$$

In Eq. 2 E_{ex} is the interconfigurational excitation energy and T_{sf} defines a width of all sublevels of two configurations. To perform such a fit $\chi(T)$ of $Y_{0.05}Ce_{0.95}CrB_4$ has to be additionally corrected on magnetic impurities (upturn for $T < 100$ K) and on paramagnetism due to conduction-electrons. The terms for such corrections are $\chi_{imp}(T) = C_{imp}/(T - \theta_{imp})$ and χ_0, respectively. Finally, the magnetic susceptibility of the studied boride is given as:

$$\chi(T) = \chi_{ICF}(T) + \chi_{imp}(T) + \chi_0 \quad (3)$$

A fit to Eq. 3 (inset a to Fig. 6) results in E_{ex}/k_B = 1747(24) K; T_{sf} = 594(11) K; C_{imp} = 5.4(1) $\times 10^{-3}$ emu K mol^{-1}; θ_{imp} = -17.4(8) K and χ_0 = 1.22(6) $\times 10^{-4}$ emu K mol^{-1}. Then, the average valence of Ce atoms in $Y_{0.05}Ce_{0.95}CrB_4$ is estimated as $\nu_{ICF} = 4n_{eff} + 3(1 - n_{eff})$. The so calculated ν_{ICF} = +3.54 at RT is in excellent agreement with the value deduced from XAS.

The close values of Ce-valences in $CeCrB_4$ and $Y_{0.05}Ce_{0.95}CrB_4$ obtained from XAS and the much stronger magnetism of the undoped ternary Ce-boride indicated a contribution of an additional paramagnetic impurity phase (e.g. CrB_2). To estimate its order of magnitude we subtracted $\chi(T)$ of the sample with $x = 0.95$ from this of $x = 1$ and fit the obtained difference to a CW law. The fit resulted in 4.1 % of impurity and a small negative Weiss temperature $\theta_P = -6$ K (Fig. S6). Subtraction of this CW-part from $\chi(T)$ of $CeCrB_4$ resulted in a well pronounced maximum comparable with this of $Y_{0.05}Ce_{0.95}CrB_4$ and is reminiscent of the CS-model for a $J = 3/2$ multiplet (inset to Fig. S6) with characteristic temperature T_0 = 867 K. Estimating the Kondo temperature in the same way as described above results in T_K = 727 K and is by a factor of about 2 smaller than this of $Y_{0.05}Ce_{0.95}CrB_4$. However, such a comparison is tentative, since the exact amount of the paramagnetic impurity in $CeCrB_4$ is unknown. Nevertheless, T_K obtained from this estimation is still well above RT and agrees well with the simple metallic properties of the ternary boride.

E. Electrical transport properties

The temperature dependent electrical resistivities for $Y_{1-x}Ce_xCrB_4$ borides are presented in Fig. 7. Increase of Ce-content x in this series leads to the reduction of $\rho(T)$ by a factor of ∼20 and thus, to a change of the character of conductivity from a semi-metallic to a metallic one. The temperature dependence of the resistivity of $YCrB_4$ (HT range is in good agreement with an earlier report [11]) shows a rather complex behavior revealing a sharp minimum centered at ∼50 K and a broad maximum at ∼450 K followed by an activation like decrease in $\rho(T)$, as expected for semiconductors. Such a behavior is reminiscent of those of Ag_xTiSe_2 [42], $TiSe_2$ [43], $ZrTe_5$ [44] or $RhSb_2$ [45] narrow gap semiconductors as well as of bad metals e.g. some rare-earth containing Heusler compounds [46] and for the strongly disordered $Ca_3Pt_{4+x}Ge_{13-y}$ Remeika phase [47]. In most the cases it is however less understood. The broad peak in resistivity of $TiSe_2$ centred at ∼165 K is explained with a crossover between a low-temperature regime with electron-like carriers only, to a regime around room temperature where thermally activated and highly mobile hole-like carriers dominate the conductivity [43].

Taking into account, that $\rho(T)$ of semiconductors is highly sensitive to the presence of impurities this prompted us to perform additional characterization of the sample after physical properties measurements. XRD and EDX revealed it to be partially inhomogeneous and to contain small amounts of YB_2, Cr_3B_4 and CrB_2 phases (Fig. S4).

Small doping of $YCrB_4$ with Ce (*i.e.* $Y_{0.95}Ce_{0.05}CrB_4$) leads to a reduction of $\rho(T)$ (*i.e.* more metallic character of conducting mechanism) and to a remarkable suppression of the broad maximum with simultaneous shift of its centre towards higher temperatures (∼550 K). Both $\rho(T)$ for $Y_{0.05}Ce_{0.95}CrB_4$ and $CeCrB_4$ are almost identical [$\rho(T)$ is slightly higher for the Y-containing compound, which is in agreement with a common tendency in the whole $Y_{1-x}Ce_xCrB_4$ series] and increase with increasing temperature in the whole range. The absence of a Kondo-like minimum in $\rho(T)$ of $Y_{0.05}Ce_{0.95}CrB_4$ confirms again the Kondo-temperature T_K to be higher than 800 K (in agreement with T_K= 1107 K deduced from analysis of the magnetic susceptibility).

The temperature dependence of electrical resistivity of IV systems is expected to follow a $\sim T^2$ law (*i.e.* Fermi liquid behavior due to the paramagnon picture [48]), as it is the case for *e.g.* $Ce_{0.5}Eu_{0.5}Pd_3$ [49], $Ce_2Rh_3Al_9$ [50], $CeNiSi_2$ [51], $Ce_2Co_3Ge_5$ [52], $CeIr_2Zn_{20}$ [53] *etc.*. However, also IV systems revealing a well pronounced metallic character of $\rho(T)$ dependences have been reported to exist. For instance, electrical resistivity is found to be linear in the higher temperature range for $CeRh_6Si_4$ [54]. For $YbCu_4In$ [55] it could be fitted to a sum of $(\rho_0 + AT^2)$- (indicating evolution of the Fermi-liquid state) and a T^5-term (suggesting a conventional electron-phonon scattering mechanisms). In the case of CeB_4 [56] the electri-

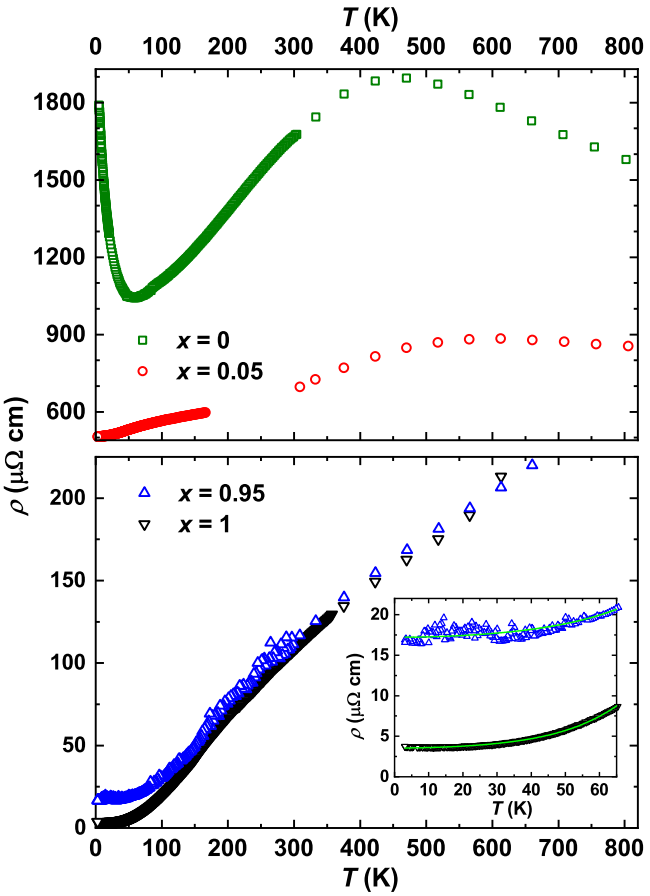

FIG. 7. (Color online) Temperature dependence of the electrical resistivity of $Y_{1-x}Ce_xCrB_4$ borides. Inset: low temperature region of the electrical resistivity of $x = 1$ and $x = 0.95$ compounds together with fits to the sum of T^2- and T^5-terms (green lines).

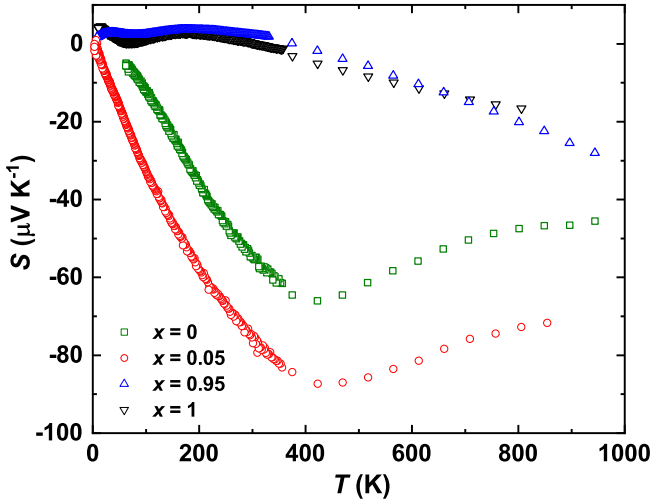

FIG. 8. (Color online) Temperature dependence of the thermopower for $Y_{1-x}Ce_xCrB_4$.

cal resistivity can be described by the Bloch-Grüneisen equation. $\rho(T)$ of $Y_{0.05}Ce_{0.95}CrB_4$ and $CeCrB_4$ in the temperature range up to 250 K can be described by a sum of of T^2- and T^5-terms confirming a scenario where the electron-phonon scattering plays an important role in their conduction mechanisms.

The calculated residual resistivity ratios ($RRR = \rho^{300}/\rho_0$) (Table I) show the ternary $CeCrB_4$ boride to be of much better quality than doped the $Y_{0.05}Ce_{0.95}CrB_4$, which can be explained by additional structural disorder in the latter sample.

The temperature variations of the Seebeck coefficient, $S(T)$, for the $Y_{1-x}Ce_xCrB_4$ series are depicted in Fig. 8. In common they show the same trend as those observed for electrical resistivities (*i.e.* increase of Ce-content x leads to more pronounced metallic properties) in agreement with the relation between $S(T)$ and $\rho(T)$ [i.e. $S = (8\pi^2 k_B^2/3eh^2)m^*T(e\pi\mu\rho/3)^{2/3}$, where m^* is effective mass and μ is the charge carriers mobility] [57]. Also, the $Y_{1-x}Ce_xCrB_4$ series shows negative values of $S(T)$ (with exception for both Ce-rich compounds which reveal small positive values of $S \leq 3\,\mu$V K^{-1} for $T < 300$ K) implying predominance of electron-type charge carriers in the studied borides.

The $S(T)$ data of $YCrB_4$ and $Y_{0.95}Ce_{0.05}CrB_4$ reveal well pronounced minima centred at ∼400 K. Similar temperature behaviour of the Seebeck coefficients is reported for numerous semiconductors. Typical examples are Si ($T_{min} \approx 180$ K) [58], $FeGa_3$ ($T_{min} \approx 20$ K) [59], In_2S_3 ($T_{min} \approx 180$ K) [60], $In_{0.74}(In_{1.8}Fe_{0.2})S_4$ ($T_{min} \approx 300$ K) [61] *etc.* A low temperature minimum/maximum (T_{min} is normally lower than $\theta_D/3$) preceded by a drastic increase/decrease of S is normally a signature of the phonon-drag effect [62] (evidenced for Si [58] and $FeGa_3$ [59]). The origin of such a high-temperature behaviour of $S(T)$ is less clear. Since intermetallic borides are known to be very hard materials and to possess high melting points [63, 64] one could expect high Debye temperatures for $YCrB_4$ and $Y_{0.95}Ce_{0.05}CrB_4$. From theoretical calculation a value $\theta_D = 965$ K is given in Ref. [9]. Thus, a phonon-drag scenario is very likely in this case.

$Y_{0.05}Ce_{0.95}CrB_4$ and $CeCrB_4$ reveal small Seebeck coefficients, which decrease almost linearly with increasing temperature as expected for metals. However, these values are by 2-3 orders of magnitude smaller than those observed for good thermoelectrics [5].

The efficiency of electrical transport properties for possible thermoelectric applications is estimated as power factor $PF = S^2/\rho$. The maximal values of PF at a certain temperature for the $Y_{1-x}Ce_xCrB_4$ series are listed in Table I. They are small in comparison with those expected for a good TE material [5] and of the same order of magnitude as those previously reported for $YCrB_4$ in Ref.[11]. The modest PF-values can be explained by enhanced electrical resistivity in Y-rich borides and small Seebeck coefficients in the Ce-rich compounds.

F. Thermal conductivity

The thermal conductivity $\kappa(T)$ of $Y_{1-x}Ce_xCrB_4$ is relatively large even at higher temperatures (Fig. 9a) and of the same order of magnitude as those observed for isostructural $TmAlB_4$ [65] and $RReB_4$ [30] borides. Also, all of them are characterized by well pronounced maxima in $\kappa(T)$ centred at ∼50-80 K and by nearly the same temperature independent value of $\kappa \approx 10$ W m^{-1} K^{-1} for $T > 400$ K range (Fig. 9a). The presence of low temperature maxima in the thermal conductivities of $Y_{1-x}Ce_xCrB_4$ borides confirm them to be well crystallized (see Fig. S3) and to contain less impurities [66].

The electronic contribution to the thermal conductivity is calculated from the Wiedemann-Franz equation: $\kappa_{el} = L_0T/\rho(T)$ (Lorenz number $L_0 = 2.44 \times 10^{-8}$ W Ω K^{-2}). As one can see from the inset in Fig. 9a, κ_{el} dominates $\kappa(T)$ of Ce-rich borides (*i.e.* $CeCrB_4$ and $Y_{0.05}Ce_{0.95}CrB_4$). For $YCrB_4$ and $Y_{0.95}Ce_{0.05}CrB_4$ κ_{el} is negligibly small. Thus here the phononic contribution given as $\kappa_{ph} = \kappa - \kappa_{el}$ is prevailing (Fig. 9b). Such a behaviour agrees well with the semiconducting nature of the Y-rich borides [a maximum in $\kappa(T)$ is of phononic origin] and the metallicity of the Ce-rich ones (κ_{el} is characterized by a maximum). In the low temperature range (10-30 K) the phononic thermal conductivities of all samples (inset to Fig. 9b) reveal a linear T-dependence, indicating κ_{ph} to be dominated by point-defect scattering mechanisms [66, 67]. A behaviour of κ_{ph} proportional to T^3, which corresponds to the dominance of grain-boundary scattering, is only visible in the 3-8 K range for the $Y_{0.05}Ce_{0.95}CrB_4$ boride. Finally, the high temperature κ_{ph} ($T > 400$ K) is proportional to T^{-1} for all borides studied here (inset to Fig. 9b), which indicate the *umklapp* processes to dominate the phonon scattering there [66].

The thermal conductivities of the $Y_{1-x}Ce_xCrB_4$ series are by approximately two orders of magnitudes larger than those of good thermoelectric materials ($\kappa < 5$ W m^{-1} K^{-1}) [68]. Thus, the large values of $\kappa(T)$ together with small Seebeck coefficients of thermopower $S(T)$ result in poor thermoelectric performance of our $Y_{1-x}Ce_xCrB_4$ series: the highest dimensionless figure of merit $ZT = 0.06$ ($ZT \approx 1$ is expected for the state-of-the-art materials) is observed for $Y_{0.95}Ce_{0.05}CrB_4$ at 800 K. This is an observation which is also reported for other borides with related crystal structures [69].

This low ZT value should be close to a single crystal measurement because of the large grain size of a few hundred micrometers for our samples (see Fig. S3) It is well known that crystal imperfections and defects, including grain boundaries, scatter phonons much better than electrons, which should result in the lowering of the thermal conductivity and thus, leads to higher ZT values [70, 71, 72].

Even more, despite the grain boundaries are expected to act as obstacles against the asymmetric thermal diffusion of charge carriers from which the Seebeck effect originates, in some cases an enhancement of $|S|$ for fine polycrystalline samples in comparison with single crystals has been reported [73, 74].

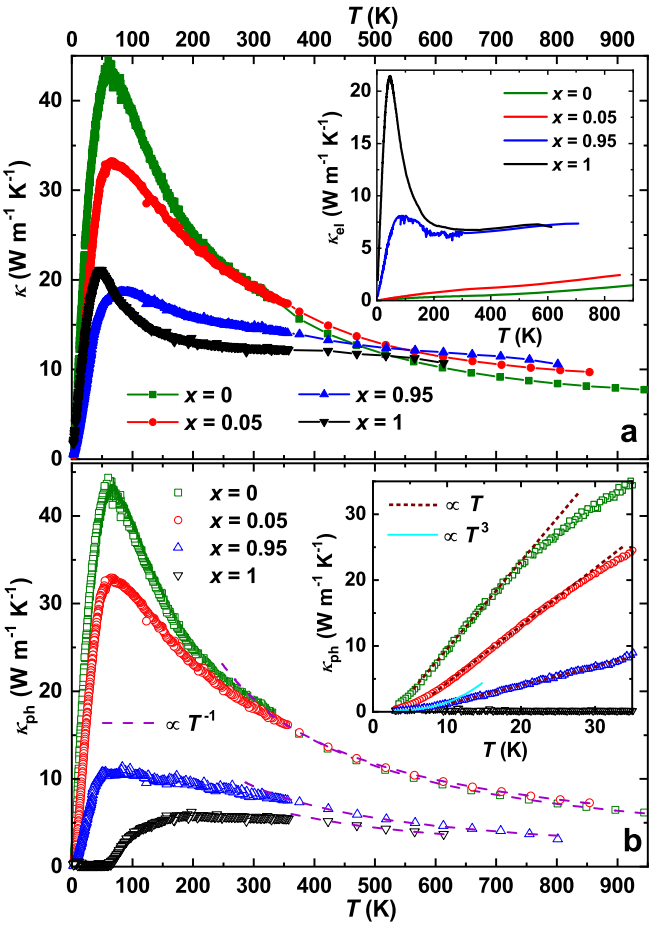

FIG. 9. (Color online) Temperature dependence of (a) the total thermal conductivities κ, electronic thermal conductivity κ_{el} (inset in a) and phononic contributions κ_{ph} (b and in inset therein) for $Y_{1-x}Ce_xCrB_4$.

It can be expected that an introduction of an array of grain boundaries in $Y_{1-x}Ce_xCrB_4$ (e.g. by spark plasma sintering of fine powdered samples) could improve their TE performance. However, a technical application of $Y_{1-x}Ce_xCrB_4$ as thermoelectric material seems not likely.

IV. SUMMARY AND CONCLUSIONS

Stimulated by density functional calculation results regarding the semiconducting or metallic nature of $YCrB_4$ and $CeCrB_4$, we studied a quaternary substitution series of $Y_{1-x}Ce_xCrB_4$ experimentally targeting their possibly promising thermoelectric properties. Like in $CePd_3$ [12], electron correlation effects from the insertion of Ce were anticipated to lead to a strongly enhanced Seebeck coefficient and a sizeable figure of merit. Together

with its intrinsic refractory and chemical inert properties, $Y_{1-x}Ce_xCrB_4$ could have been an attractive material for high temperature applications.

In contrast to expectations, from combined X-ray diffraction and energy dispersive - or wavelength dispersive spectrometry (EDXS/WDXS) studies, we find that the stability range of $Y_{1-x}Ce_xCrB_4$ is rather narrow and only a limited solid solution is formed. We obtain only samples on the Y- and Ce-rich substitution limits, comprising a maximum of 5% of the respective substituents (x = 0, 0.05, 0.95, 1). The significant size mismatch of Y and Ce-ions (being in an intermediate valence state) most probably causes such behaviour.

Doping of $YCrB_4$ with Ce leads to a strong reduction of the resistivity. Whereas the Y-rich $Y_{0.95}Ce_{0.05}CrB_4$ still shows a broad maximum at higher temperatures and sizeable resistivity at low temperatures, the Ce-rich substituents show pronounced metallic character (see Fig. 7). X-ray absorption spectroscopy (XAS) revealed Ce-atoms to be in nearly the same oxidation state of about +3.5 (see Fig. 5) throughout the series $Y_{1-x}Ce_xCrB_4$ (x = 0.05, 0.95, 1).

For the Ce-rich compounds (x = 0.95, 1), the intermediate Ce valence concluded from XAS is in good agreement with the measured magnetic susceptibilities (see Fig. 6). A broad maximum in the magnetic susceptibility of both materials (after subtraction of a paramagnetic impurity for x = 1) is described by the Kondo-model of Coqblin and Schrieffer (see insets in Fig. 6 and Fig. S6). A quantitative analysis yields a Kondo-temperature T_K= 1107 K (for x =0.95) which is about 4 times higher than T_K = 300 K of the intermetallic thermoelectric $CePd_3$. Applying a simplified two-level interconfiguration fluctuation model, the slightly temperature dependent intermediate valence of Ce (+3.54) is in line with the observations from XAS at room temperature.

The absolute thermopower values for the Y-rich $Y_{0.95}Ce_{0.05}CrB_4$ and $YCrB_4$ compounds are rather large and are passing through broad maxima. However, the thermopower for the Ce-rich $Y_{0.05}Ce_{0.95}CrB_4$ and $CeCrB_4$ borides is small with a slight increase for the high temperature range. Thus, in contrast to the motivation of our study, the electron correlation effects for the Ce -rich materials do not influence significantly the transport properties of these systems. This can be explained by their extremely high Kondo-temperature.

The $Y_{1-x}Ce_xCrB_4$ (x = 0, 0.05, 0.95, 1) series reveals an unexpectedly good thermal conductivity. Both ternaries show well pronounced maxima at about 70 K and 45 K, respectively, which become suppressed with incorporation of the fourth component because of structural disorder. Also, the mechanism of the thermal conductivity is predominantly electronic in Ce-rich borides and predominantly phononic for the Y-rich $Y_{0.95}Ce_{0.05}CrB_4$ and $YCrB_4$. Finally, the good thermal conductivity in the $Y_{1-x}Ce_xCrB_4$ series results in a poor thermoelectric performance with a dimensionless figure-of-merit ZT = 0.06 at 800 K.

Although the here applied concept of Ce-substitution in $YCrB_4$ to obtain materials with high thermoelectric performance was not successful, the accompanying DFT calculations revealed an unusual and interesting feature in the electronic structure of the parent compound $YCrB_4$. Besides yielding semiconducting behavior with a narrow indirect gap (∼140 meV for the experimental B positions, see Fig. 1) and metallic behavior for the $CeCrB_4$ (in the limit of fully localized $4f$ electrons, see Fig. S1), the electronic densities of states are characterized by narrow peaks near the Fermi level. These singularities are predominantly from the Cr $3d_{z^2-r^2}$ orbitals and have a pronounced quasi one-dimensional character (see Fig. 2). Although the electronic band structure of $YCrB_4$ is very sensitive to the B-B distances in the crystal structure, these van-Hove like singularities should therefore be rather robust. A small amount of electron doping should shift the Fermi level upwards into the lower lying narrow peak and, due to its very high DOS, most likely cause an electronic instability. Since a partial substitution of Y by Ce is not suitable for this purpose (due to its intermediate valence of about +3.5 as this work has demonstrated), a study of alternative substitution is presently executed.

ACKNOWLEDGMENTS

This work was performed within DFG project 324961605. The authors are grateful to M. Eckert, P. Scheppan, and S. Kostmann for their help during the metallographic investigations. We express our thanks to H. Borrmann and S. Hückmann for performing X-ray diffraction measurements. U. Nitzsche is acknowledged for technical support of the calculations. We thank E. Zuniga and P. Wyżga for their assistance during high-temperature electrical transport measurements and Yu. Grin for his interest.

* roman.gumeniuk@physik.tu-freiberg.de

[1] J. Sommerlatte, K. Nielsch, and H. Böttner, Phys. J. **6**, 35 (2007), URL https://www.pro-physik.de/physik-journal/mai-2007.

[2] L.-D. Zhao, V. P. Dravid, and M. G. Kanatzidis, Energy Environ. Sci. **7**, 251 (2014).

[3] T. Mori, J. Phys.: Conf. Series **176**, 012036 (2009).

[4] T. Mori, in *Handbook on the Physics and Chemistry of Rare Earths*, edited by K. Gschneidner, J. Bünzli, and V. Pecharsky (Elsevier, 2008), vol. 38, pp. 105–173.

[5] G. Nolas, J. Sharp, and J. Goldsmid, *Thermoelectrics: Basic Principles and New Materials Developments* (Springer,

Berlin-Heidelberg, 2001).
[6] Y. B. Kuz'ma, Sov. Phys. Crystallogr. **15**, 312 (1970).
[7] Y. B. Kuz'ma, *Crystal Chemistry of Borides* (Vyshcha Shkola, Lviv, 1983).
[8] N. Medvedeva, Y. Medvedeva, and A. Ivanovskii, Doklady Phys. Chem. **383**, 75 (2002).
[9] A. Candan, G. Surucu, and A. Gencer, Physica Scripta **94**, 125710 (2019).
[10] C. Benndorf, M. de Oliveira, C. Doerenkamp, F. Haarmann, T. Fickenscher, J. Ksters, H. Eckert, and R. Pttgen, Dalton Trans. **48**, 1118 (2019).
[11] J. Simonson and S. Poon, J. Alloys Compd. **504**, 265 (2010).
[12] S. N. Mishra, J. Phys.: Cond. Matter **15**, 5333 (2003).
[13] V. R. Fanelli, J. M. Lawrence, E. A. Goremychkin, R. Osborn, E. D. Bauer, K. J. McClellan, J. D. Thompson, C. H. Booth, A. D. Christianson, and P. S. Riseborough, J. Phys.: Cond. Matter **26**, 225602 (2014).
[14] P. Sarode, D. Sarma, C. Rao, E. Sampathkumaran, L. Gupta, and R. Vijayaraghavan, Mater. Res. Bull. **16**, 175 (1981).
[15] G. Mahan and M. Bartowiak, Acta Phys. Pol. A **97**, 37 (2000).
[16] R. Gumeniuk, W. Schnelle, K. O. Kvashnina, and A. Leithe-Jasper, J. Phys.: Cond. Matter **28**, 165603 (2016).
[17] Y. B. Kuz'ma, S. I. Svarichevskaya, and F. V. N., Inorg. Mater. USSR **9**, 1372 (1973).
[18] STOE Powder Software, WinXPow (version 2), Darmstadt, STOE and Cie GmbH, 2001.
[19] L. Akselrud and Y. Grin, J. Appl. Crystallogr. **47**, 803 (2014).
[20] K. O. Kvashnina and A. C. Scheinost, J. Synchrotron Rad. **23**, 836 (2016).
[21] K. Koepernik and H. Eschrig, Phys. Rev. B **59**, 1743 (1999).
[22] J. P. Perdew, K. Burke, and M. Ernzerhof, Phys. Rev. Lett. **77**, 3865 (1996).
[23] A. Iandelli and A. Palenzona, in *Alloys and Intermetallics* (Elsevier, 1979), vol. 2 of *Handbook on the Physics and Chemistry of Rare Earths*, pp. 1–54.
[24] L. Vegard, Z. Kristallogr. **67**, 239 (1928).
[25] A. R. Denton and N. W. Ashcroft, Phys. Rev. A **43**, 3161 (1991).
[26] W. Hume-Rothery and G. V. Raynor, The London, Edinburgh, and Dublin Philosophical Magazine and Journal of Science **26**, 143 (1938).
[27] L. S. Darken and R. W. Gurry, in *Physical Chemistry of Metals*, edited by R. F. Mehl (McGrawHill Book Comp., 1953), Metallurgy and Metallurgical Engineering Series, pp. 1–595.
[28] J. T. Waber, K. G. Jr., A. C. Larson, and M. Y. Prince, Trans. Metall. Soc. AIME **227**, 717 (1963).
[29] K. A. Gschneidner and M. Verkade, Progr. Mater. Sci. **49**, 411 (2004), a Festschrift in Honor of T. B. Massalski.
[30] M. Abramchuk, W. Schnelle, I. Veremchuk, A. Leithe-Jasper, Y. Grin, and R. Gumeniuk, Eur. J. Inorg. Chem. **2016**, 161 (2016).
[31] I. Veremchuk, T. Mori, Y. Prots, W. Schnelle, A. Leithe-Jasper, M. Kohout, and Y. Grin, J. Solid State Chem. **181**, 1983 (2008).
[32] J. Emsley, *The Elements* (Clarendon Press, Oxford, 1998).
[33] J. Lawrence, Phys. Rev. B **20**, 3770 (1979).
[34] J. R. Thomson, S. T. Sekula, C.-K. Loong, and C. Stassis, J. Appl. Phys. **53**, 7893 (1982).
[35] V. T. Rajan, Phys. Rev. Lett. **51**, 308 (1983).
[36] I. Aviani, M. Miljak, V. Zlatić, K.-D. Schotte, C. Geibel, and F. Steglich, Phys. Rev. B **64**, 184438 (2001).
[37] H. Michor, K. Kreiner, N. Tsujii, K. Yoshimura, K. Kosuge, and G. Hilscher, Phys. B: Cond. Matter **319**, 277 (2002).
[38] H. Yamaoka, N. Tsujii, Y. Utsumi, H. Sato, I. Jarrige, Y. Yamamoto, J.-F. Lin, N. Hiraoka, H. Ishii, K.-D. Tsuei, et al., Phys. Rev. B **87**, 205120 (2013).
[39] A. P. Murani, W. C. M. Mattens, F. R. de Boer, and G. H. Lander, Phys. Rev. B **31**, 52 (1985).
[40] J. W. Rasul and A. C. Hewson, J. Phys. C: Solid State Phys. **17**, 2555 (1984).
[41] B. Sales and D. Wohlleben, Phys. Rev. Lett. **35**, 1240 (1975).
[42] L. Krasavin, A. Titov, and V. Antropov, Phys. Solid State **40**, 1962 (1998).
[43] M. D. Watson, A. M. Beales, and P. D. C. King, Phys. Rev. B **99**, 195142 (2019).
[44] S. A. Miller, I. Witting, U. Aydemir, L. Peng, A. J. E. Rettie, P. Gorai, D. Y. Chung, M. G. Kanatzidis, M. Grayson, V. Stevanović, et al., Phys. Rev. Applied **9**, 014025 (2018).
[45] D. S. Wu, Y. T. Qian, Z. Y. Liu, W. Wu, Y. J. Li, S. H. Na, S. Y. T., P. Zheng, G. Li, J. G. Cheng, et al., Chinese Phys. B **29**, 037101 (2020).
[46] D. Kaczorowski, K. Gofryk, T. Plackowski, A. Leithe-Jasper, and Y. Grin, J. Magn. Magn. Mater. **290–291**, 573 (2005), proceedings of the Joint European Magnetic Symposia (JEMS' 04).
[47] R. Gumeniuk, L. Akselrud, K. O. Kvashnina, W. Schnelle, A. A. Tsirlin, C. Curfs, H. Rosner, M. Schoneich, U. Burkhardt, U. Schwarz, et al., Dalton Trans. **41**, 6299 (2012).
[48] J. M. Lawrence, P. S. Riseborough, and R. D. Parks, Rep. Prog. Phys. **44**, 1 (1981).
[49] A. Pandey, C. Mazumdar, R. Ranganathan, V. R. Reddy, and A. Gupta, Appl. Phys. Lett. **94**, 182503 (2009).
[50] M. Falkowski and A. Strydom, J. Low Temp. Phys. **175**, 498 (2014).
[51] E. D. Mun, Y. S. Kwon, and M. H. Jung, Phys. Rev. B **67**, 033103 (2003).
[52] S. Layek, V. Anand, and Z. Hossain, J. Magn. Magn. Mater. **321**, 3447 (2009).
[53] P. Swatek and D. Kaczorowski, J. Phys.: Cond. Matter **25**, 055602 (2013).
[54] T. Gruner and C. Geibel, in *Solid Compounds of Transition Elements* (Trans Tech Publications Ltd, 2017), vol. 257 of *Solid State Phenomena*, pp. 199–202.
[55] N. Tsujii, K. Yoshimura, and K. Kosuge, J. Phys.: Cond. Matter **15**, 1993 (2003).
[56] V. Babizhetskyy, A. Simon, and K. Hiebl, Z. Naturforsch. B **62**, 896 (2007).
[57] M. Cutler and N. F. Mott, Phys. Rev. **181**, 1336 (1969).
[58] T. H. Geballe and G. W. Hull, Phys. Rev. **98**, 940 (1955).
[59] M. Wagner-Reetz, D. Kasinathan, W. Schnelle, R. Cardoso-Gil, H. Rosner, Y. Grin, and P. Gille, Phys. Rev. B **90**, 195206 (2014).
[60] P. Wyzga, I. Veremchuk, C. Himcinschi, U. Burkhardt, W. Carrillo-Cabrera, M. Bobnar, C. Hennig, A. Leithe-Jasper, J. Kortus, and R. Gumeniuk, Dalton Trans. **48**, 8350 (2019).

[61] P. Wyzga, I. Veremchuk, M. Bobnar, P. Kozelj, S. Klenner, R. Poettgen, A. Leithe-Jasper, and R. Gumeniuk, Chemistry A European Journal **26**, 5245 (2020).
[62] C. Kittel, *Introduction to Solid State Physics* (J. Wiley & Sons, New York, 1986), sixth edition.
[63] in *Boron and Refractory Borides*, edited by G. V. Samsonov, P. Hagenmuller, T. Lundstrom, and V. I. Matkovich (Springer-Verlag Berlin Heidelberg, 1977), pp. 1–656.
[64] G. Samsonov and I. M. Vinitskii, *Handbook of Refractory Compounds* (Springer US, 1980).
[65] X. J. Wang, T. Mori, I. Kuzmych-Ianchuk, Y. Michiue, K. Yubuta, T. Shishido, Y. Grin, S. Okada, and D. G. Cahill, APL Materials **2**, 046113 (2014).
[66] T. Tritt, *Thermal conductivity: Theory, Properties and Applications* (Springer, Science and Business Media, Berlin, 2005).
[67] J. Yang, D. T. Morelli, G. P. Meisner, W. Chen, J. S. Dyck, and C. Uher, Phys. Rev. B **65**, 094115 (2002).
[68] C. Uher, in *Chemistry, Physics and Materials Science of Thermoelectric Materials: Beyond Bismuth Telluride*, edited by M. Kanatzidis, S. Mahanti, and T. Hogan (Kluwer Academics, Plenum Publishers, New York, 2003), p. 121.
[69] T. Mori, J. Solid State Chem. **275**, 70 (2019).
[70] C. Gayner and K. K. Kar, Progress in Materials Science **83**, 330 (2016).
[71] Z. Chen, B. Ge, W. Li, S. Lin, J. Shen, Y. Chang, R. Hanus, G. J. Snyder, and Y. Pei, Nature Communications **8**, 13828 (2017).
[72] X. Yan, M. Ikeda, L. Zhang, E. Bauer, P. Rogl, G. Giester, A. Prokofiev, and S. Paschen, J. Mater. Chem. A **6**, 1727 (2018).
[73] S. Walia, S. Balendhran, H. Nili, S. Zhuiykov, G. Rosengarten, Q. H. Wang, M. Bhaskaran, S. Sriram, M. S. Strano, and K. Kalantar-zadeh, Progress in Materials Science **58**, 1443 (2013).
[74] S. I. Kim, K. H. Lee, H. A. Mun, H. S. Kim, S. W. Hwang, J. W. Roh, D. J. Yang, W. H. Shin, X. S. Li, Y. H. Lee, et al., Science **348**, 109 (2015).